Tuning the 3D plasmon field of nanohole arrays

Maxime Couture[1], Yuzhang Liang[2], Hugo-Pierre Poirier Richard[1], Rita Faid[1], Wei Peng[2] and Jean-Francois Masson[1,3]*

[1] Département de chimie, Université de Montréal, CP. 6128 Succ. Centre-Ville, Montréal, Qc, Canada, H3C 3J7

[2] College of Physics and Optoelectronics Engineering, Dalian University of Technology, Dalian, 116024, China

[3] Centre for self-assembled chemical structures (CSACS)

* Contact information: email: jf.masson@umontreal.ca ; Tel: +1-514-343-7342

Supporting information

Derivation of the SPP equation for nanohole arrays

$$k_{spp} = k_{light}; \quad \frac{\omega}{c} \sqrt{\frac{\varepsilon_m \varepsilon_d}{\varepsilon_m + \varepsilon_d}} = \left| n_D k_0 sin\theta + iG_x + jG_y + lG_z \right| \qquad (1)$$

where ω is the angular frequency, c the speed of light, ε_d and ε_m are the real dielectric constants of the dielectric and the metal respectively, n_D is the refractive index of the medium in which light propagates, G_x, G_y and G_z corresponds to Bragg vectors, and k_0 the momentum of free-space light at a specific angle of incidence (θ). BW-SPPs modes are characterized by the integers i, j and l representing the orders of diffraction that couple with the incident light.
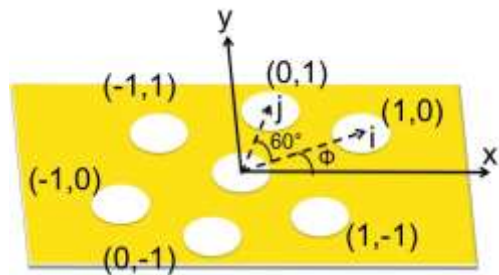
Figure SI1. Schematic representation of the BW-SPPs modes and azimuthal angle (ϕ).

Wavevector matching conditions for excitation of the SPP for nanohole arrays:

$$k_{spp} = k_o\, n_D\, \sin\theta\,(x+y) + i\, Gx + j\, Gy \qquad (2)$$

$$k_{spp} = \frac{2\pi}{\lambda}\sqrt{\frac{\varepsilon_m \varepsilon_d}{\varepsilon_m + \varepsilon_d}} \qquad (3)$$

$$k_o = \frac{2\pi}{\lambda} \qquad (4)$$

Where x and y are the projection of the modes (i,j) in the x and y axis (see figure SI1).

The projection of the (i,j) mode is:

For hexagonal arrays of nanoholes:

$$x = i\cos(\phi) + j\,\cos(\phi + 60) \qquad (5)$$

$$y = i\sin(\phi) + j\,\sin(\phi + 60) \qquad (6)$$

For square arrays of nanoholes:

$$x = i\cos(\phi) + j\,\cos(\phi + 90) \qquad (7)$$

$$y = i\sin(\phi) + j\,\sin(\phi + 90) \qquad (8)$$

The Bragg vectors are:

For hexagonal arrays of nanoholes:

2

$$G = \frac{4\pi}{\sqrt{3}\,P} \tag{9}$$

For square arrays of nanoholes:

$$G = \frac{2\pi}{P} \tag{10}$$

Rearranging equations 1-10

Thus, at normal incidence and with no azimuthal rotation of the sample, we get the original equation of nanohole arrays:

For hexagonal arrays of nanoholes:

$$\lambda = \frac{P}{\sqrt{\frac{4}{3}(i^2 + ij + j^2)}} \left(\sqrt{\frac{\varepsilon_m \varepsilon_d}{\varepsilon_m + \varepsilon_d}} \right) \tag{11}$$

For square arrays of nanoholes:

$$\lambda = \frac{P}{\sqrt{(i^2 + j^2)}} \left(\sqrt{\frac{\varepsilon_m \varepsilon_d}{\varepsilon_m + \varepsilon_d}} \right) \tag{12}$$

Then, with non-zero incident angle, but with no consideration of the rotation of the sample (aligned with the (1,0) mode):

For hexagonal arrays of nanoholes:

$$\lambda = \frac{P}{\sqrt{\frac{4}{3}(i^2 + ij + j^2)}} \left(\sqrt{\frac{\varepsilon_m \varepsilon_d}{\varepsilon_m + \varepsilon_d}} - \eta_D \sin\theta \right) \tag{13}$$

For square arrays of nanoholes:

$$\lambda = \frac{P}{\sqrt{(i^2 + j^2)}} \left(\sqrt{\frac{\varepsilon_m \varepsilon_d}{\varepsilon_m + \varepsilon_d}} - \eta_D \sin\theta \right) \tag{14}$$

With non-zero incident angle and rotation of the sample:

For hexagonal arrays of nanoholes:

$$\lambda = \left(\frac{P}{\sqrt{\frac{4}{3}(i^2 + ij + j^2)}} \sqrt{\frac{\varepsilon_m \varepsilon_d}{\varepsilon_m + \varepsilon_d}} - \frac{P}{\sqrt{\frac{4}{3}(i^2 + ij + j^2)}} \eta_D \sin\theta \, (i\cos(\phi) + j\cos(\phi + 60) + i\sin(\phi) + \right.$$

$$\left. j\sin(\phi + 60)) \right) \tag{15}$$

For square arrays of nanoholes:

$$\lambda = \left(\frac{P}{\sqrt{(i^2 + j^2)}} \sqrt{\frac{\varepsilon_m \varepsilon_d}{\varepsilon_m + \varepsilon_d}} - \frac{P}{\sqrt{(i^2 + j^2)}} \eta_D \sin\theta \, (i\cos(\phi) + j\cos(\phi + 90) + i\sin(\phi) + j\sin(\phi + \right.$$

$$\left. 90)) \right) \tag{16}$$

where all angles are reported in degrees, λ is the excitation wavelength and P is the periodicity.

Referencing the transmission spectra from nanohole arrays
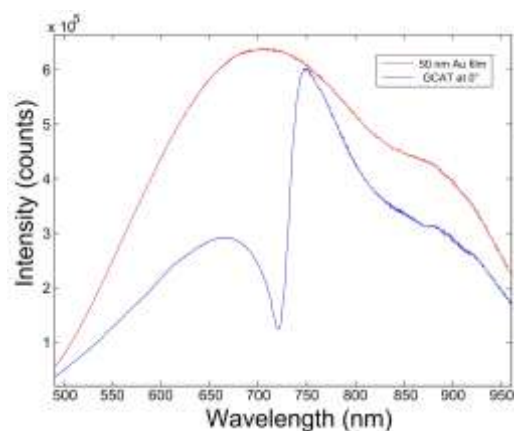
Figure SI2. Transmission spectrum of the Au film of 50 nm thickness (red) serves as a spectral reference to the transmission spectrum of Au nanohole arrays (blue).

FDTD simulation of the hole diameter and metal thickness: impacts on the plasmonic signal
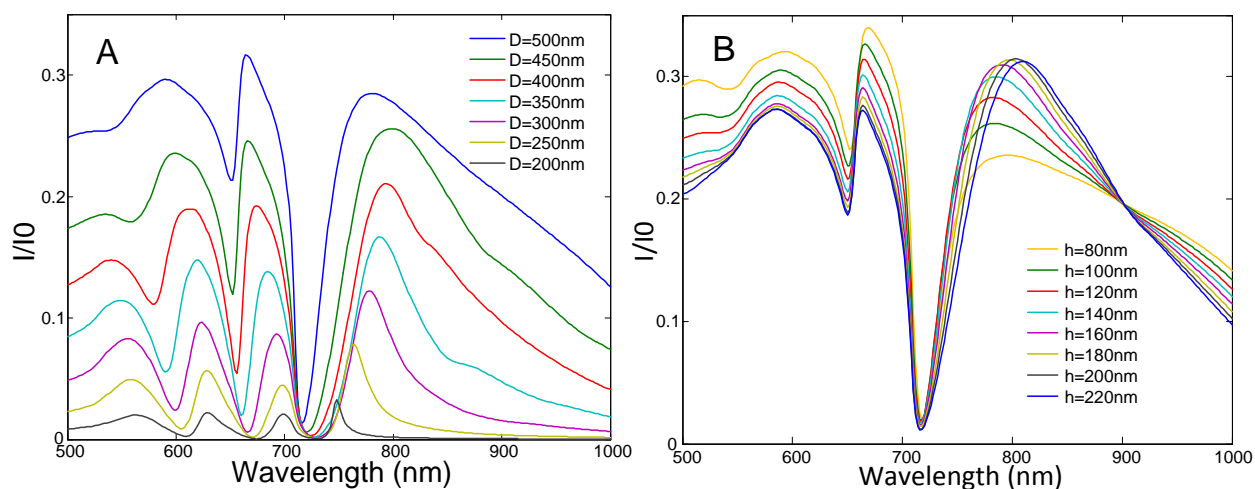
Figure SI3. FDTD simulation of the GCAT signal of gold nanohole arrays of 820 nm periodicity. A) Gold thickness of 120 nm for different hole diameter. B) Hole diameter of 500 nm for different thicknesses of Au.

Figure SI3 exposes the influence of the variation of thickness and hole diameter on the grating coupling condition at normal incidence. The GCAT signal intensity of the (1,0) mode in air weakly increases for thicker gold thicknesses. However, the augmentation of the hole diameter has an high impact on the transmission intensity of light through the hole arrays. An enhanced optical transmission was observed with small diameters of the nanoholes. With larger diameters of nanoholes, the optical properties differ greatly and the nanoholes are then mainly absorptive. Thus, figure SI3 exposes the transition from an EOT to GTAC phenomenon with larger hole diameters.

Experimental details about the fabrication of gold nanohole arrays and the optical measurements
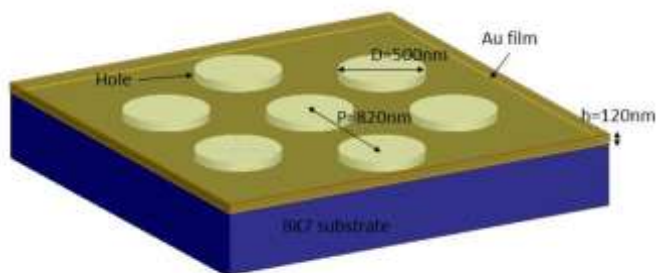
Figure SI4. Schematic representation of a gold nanohole arrays.

Gold nanohole arrays (figure SI3) were produced by a nanosphere lithography technique involving the formation of a polymer mask on a glass slides by drop-coating a solution of nanospheres with fixed diameter. Glass sides (22x22 mm^2, BK7, Fisher Scientific) were successively cleaned in piranha solution for 90 minutes and in a mixture of water, ammonia and hydrogen peroxide at a 5:1:1 ratio for 60 minutes in an ultrasonication bath. The glass slides were copiously rinsed with water between treatments and stored in ultrapure water. The polymer mask was formed by drop-coating a solution of polystyrene nanospheres (Thermo scientific particle technology) mixed with pure water (18 MΩ cm) on a clean dry glass slides. The drop-coating solution had a 5:1 ratio of water/spheres for both 820 nm and 1000 nm beads. 40 µL of the final nanospheres solution was dropped on the glass slide, evenly distributed on the surface and covered with a Petri dish until drying completion. The nanosphere lithography mask results in a hexagonal closed-packed monolayer having about 1x1 cm^2 of patterned area. Both periodicities of 820 nm or 1000 nm were treated by reactive ion etching using oxygen plasma (Harrick Plasma Cleaner PDC-32 G) at 18 W to a final sphere diameter of about 400-500 nm and 500-600 nm respectively. Thereafter, the polystyrene mask was metallized by sputtering 140 nm of Au with a 1 nm Cr adhesion layer (Cressington 308R sputter) for both periodicities. Subsequently, the polystyrene beads were removed by sonication in ethanol for 4 min, resulting in a gold nanoholes array. The optical properties were measured in transmission spectroscopy (Figure SI5).
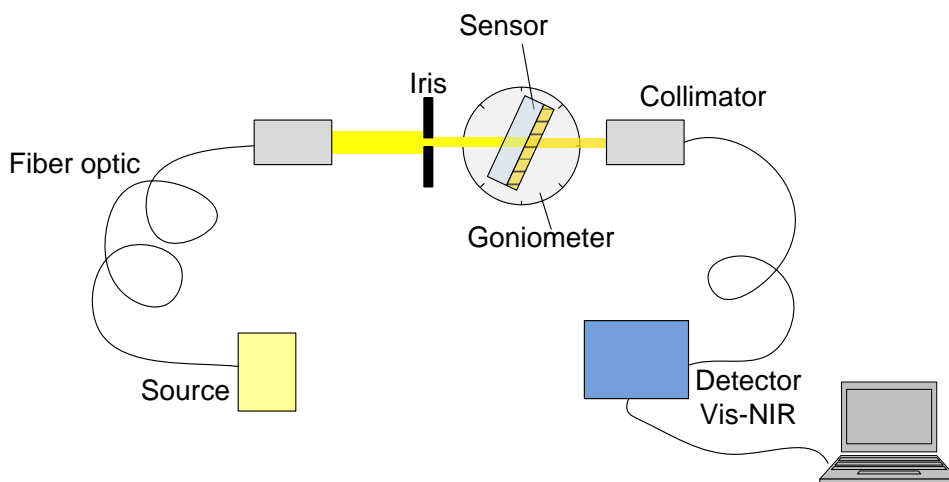
Figure SI5. Scanning angle-rotation transmission instrument. The sample (sensor) is placed on a 360 degrees rotation mount, which is fixed to a 360 degrees goniometer. A flow cell (without the azimuthal rotation capabilities) was designed with wide apertures to allow large incident angles to be investigated.

Plasmon resonance energy with incident angle and periodicity

The effect of the incident angle on the (1,0) mode of BW-SPPs mode provides intense GCAT signal covering a broad range of vis-NIR wavelengths depending on the incident angle and the periodicity of the arrays (Figure SI5). The (1,0) mode was studied for periodicities of 820 and 1000 nm with sensors of diameter/periodicity ratio (d/P) of 0.6 and 130 nm thickness. As expected from equation 1 of the main article, the position of the (1,0) Au-solution mode and the incident angle exhibit a direct relation for both periodicities of 820 and 1000 nm (figure SI5). Theoretical and experimental values in water for both periodicities are in good agreement with predictions, which is confirmed by their RSD values below 2%. Small variations between predicted and experimental values is due to the precision ($\pm 1°$) of the goniometer which is manually adjusted during experiment and small deviation of the mathematical model for the dielectric constant of Au between 550 and 650 nm due to absence of data in this range in the literature (Palik E., Handbook of optical constants of solids, Academic Press). In addition, it is expected that the actual plasmon resonance to be blue-shifted due to the existence of real holes in the metal film.
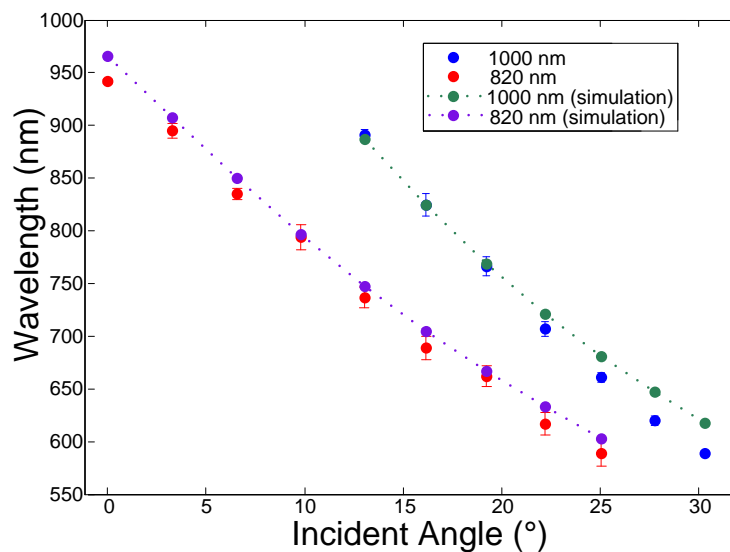
Figure SI6. Experimental and simulated (dotted) plasmon resonances of the (1,0) mode in water for gold nanohole arrays of 820 and 1000 nm of periodicity for different incident angle.
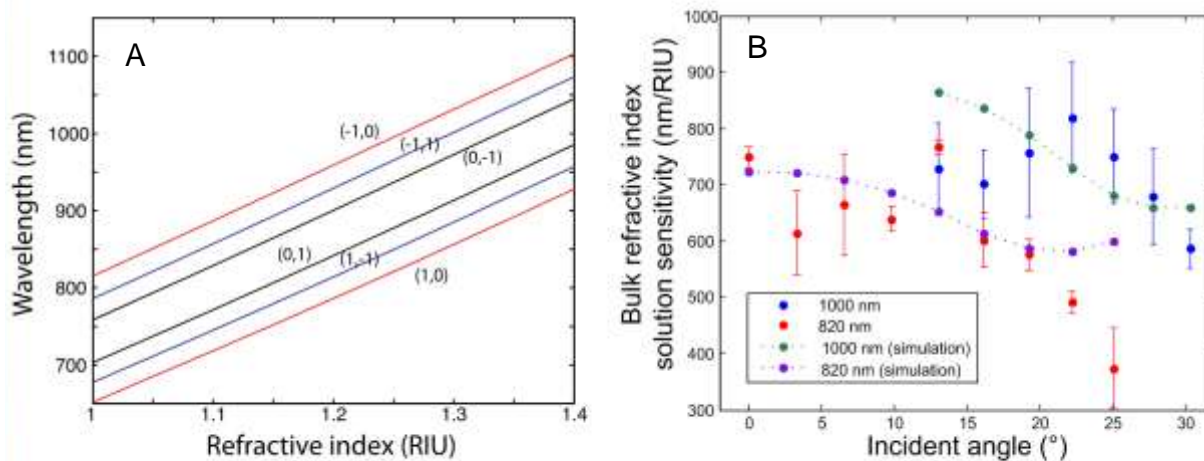
Figure SI7. A) Simulated calibration curve at 5° incident angle and 10° azimuthal rotation angle. All modes exhibit the same sensitivity for this spectral range. B) Experimental and theoretical

(dotted) bulk refractive index sensitivity of the (1,0) mode for gold nanohole arrays of 820 (red circle) and 1000 nm (blue circle) periodicity for different incident angles.

Assessing the surface sensitivity and penetration depth

While bulk refractive index sensitivity (*s*) is associated to the sensor response towards surface adsorption (surface sensitivity), the distance the field penetrates (l_d) in the solution mainly drives the surface sensitivity [1].

$$\Delta\lambda = s\Delta n \left[1 - exp\left(\frac{-2d}{l_d}\right)\right] \qquad (17)$$

where $\Delta\lambda$ is the transducer response, $\Delta\eta$ is the refractive index difference between the medium and the adsorbate layer of thickness *d*.

The LBL method exploits the adhesion of positively charged polyelectrolyte (PAH) on a negatively charged surface followed by the adhesion of a negatively charged polyelectrolyte (PSS) due to electrostatic interactions [2]. Successive adhesions of bilayers of polyelectrolytes grows thicker in a linear fashion[3,4] on a gold template[5] allowing the formation of a spacer[6] with controlled thickness. This LBL technique is well known to be simple, inexpensive and repeatable[7]. The plasmonic response associated to the adhesion of polyelectrolytes bilayers is a relevant method to probe the surface sensitivity. Figure SI8 present the average plasmonic shift associated to the adhesion of polymer bilayers (n=5) for increasing incident angle.
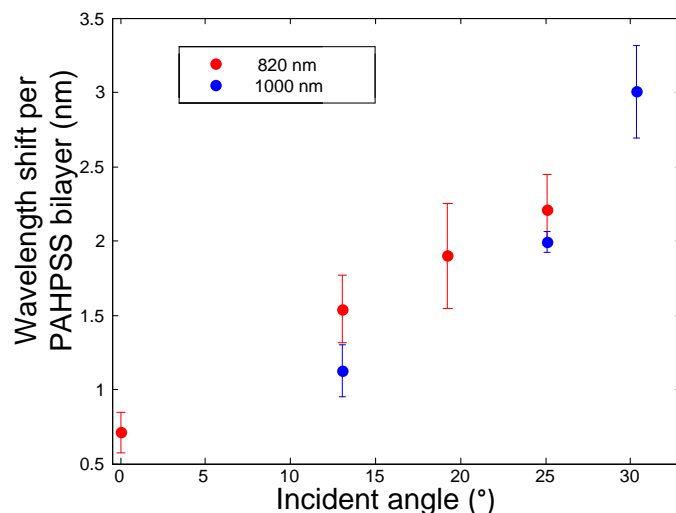
Figure SI8. Plasmonic wavelength shift of gold nanohole arrays of 820 nm (red) and 1000 nm of periodicity for the adhesion of a PAH/PSS bilayer for different incident angle.

With large thicknesses of adsorbed bilayers, the plasmonic wavelength shift should plateau due to filling of the plasmon field with polymer. Such experiment was performed for nanohole arrays of 820 nm periodicity for the (1,0) mode at incident angles of 0°, 13°, 19° and 25° (Figure SI9a). For larger incidence angles, we observed a linear region of the plasmonic shift followed by the plateau when adsorbing 30-40 bilayers. For smaller incidence angles, the number of polyelectrolyte bilayers was larger before reaching the plateau, indicating a larger sensing volume. The decay length associated to each incident angle can be estimated using equation SI17 (Figure SI9b). By analyzing the change of the plasmonic response of the nanohole arrays with increasing polyelectrolyte deposition, it was clearly observed that the decay length was decreasing for larger incident angle. It is important to note that such model used to determine the penetration depth gives approximate results. Indeed, the calculated value is dependent of the bulk refractive index sensitivity and the thickness of a bilayer upon multiple successive adsorption steps. In our case, we consider these parameters remain constant through the growth of the polymer film.

10
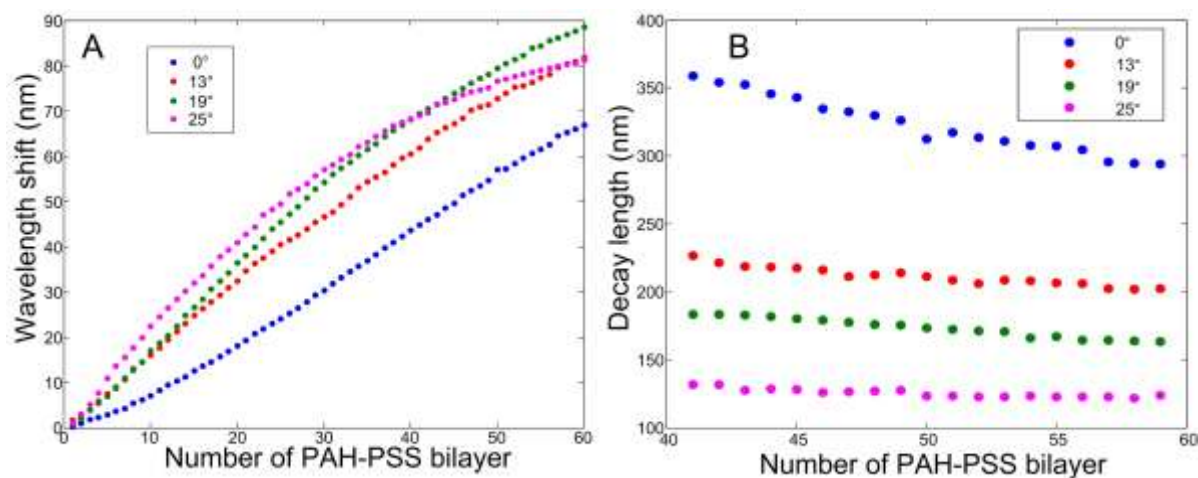
Figure SI9. a) Plasmonic wavelength shift of gold nanohole arrays of 820 nm of periodicity upon successive adsorption of 60 PAH-PSS bilayer to assess the decay length for different incident angle of 0° (blue), 13° (red), 19° (green) and 25° (pink). b) Calculated decay length for the corresponding incident angle.

References

(1) Jung, L. S.; Campbell, C. T.; Chinowsky, T. M.; Mar, M. N.; Yee, S. S. *Langmuir* **1998**, *14*, 5636.

(2) Decher, G. *Science* **1997**, *277*, 1232.

(3) Hyong-Jun Kim, K. L., Sameer Kumar, and Jinsang Kim *Langmuir* **2005**, 8532.

(4) Hoda, N.; Larson, R. G. *Journal of Physical Chemistry B* **2009**, *113*, 4232.

(5) Gittins, D. I.; Caruso, F. *Advanced Materials* **2000**, *12*, 1947.

(6) Jiang, C. Y.; Markutsya, S.; Tsukruk, V. V. *Langmuir* **2004**, *20*, 882.

(7) Von Klitzing, R.; Wong, J. E.; Jaeger, W.; Steitz, R. *Current Opinion in Colloid & Interface Science* **2004**, *9*, 158.